Research Square

Preprints are preliminary reports that have not undergone peer review.
They should not be considered conclusive, used to inform clinical practice,
or referenced by the media as validated information.

Design and development of novel organic chemosensor for rapid and selective detection of Pb^{2+} ions

Khushi Siri C N
Davangere University
Shoukat Ali R A
drsardvg2022@gmail.com
Davangere University
Latha M S
Raichur university
Madhuri R
Kirthi S Byadagi
Manjunath K

Research Article

Keywords: Azo dye, Colorimetric chemosensor, Pb^{2+} detection

Posted Date: November 24th, 2026

DOI: https://doi.org/10.21203/rs.3.rs-11657705/v1

License: This work is licensed under a Creative Commons Attribution 4.0 International License.
Read Full License

Additional Declarations: No competing interests reported.

Design and development of novel organic chemosensor for rapid and selective detection of Pb^{2+} ions.

Khushi Siri C N[1], Shoukat Ali R A[1*], Latha M S[2], Madhuri R[3], Kirthi S Byadagi[4], Manjunath k[5].

[1]Department of studies and research in chemistry, Davangere University, Shivagangotri, Davangere - 577007 Karnataka, India

[2]Department of Chemistry, Raichur University, Raichur, Karnataka, India.

[3]Department of chemistry, Govt. Engineering college, dairy circle, BM road, Hassan, Karnataka, India.

[4]Department of chemistry, KLE's Science institute (autonomous) Belagavi, Karnataka, India.

[5]Nagarjuna college of engineering and technology Bangalore-562164 Karnataka, India.

[1*]Corresponding author E-mail: drsardvg2022@gmail.com

Abstract

A series of 2-Amino5nitrobenzophenone based novel azo dyes (3a–3c) containing multifunctional donor sites were synthesized through diazotization–coupling reactions and characterized using UV–visible, FTIR, ^{1}H NMR, ^{13}C NMR, and LC–MS spectral analyses. The chemosensor behaviour of the synthesized dyes toward various metal ions including Fe^{2+}, Co^{2+}, Zn^{2+}, Hg^{2+}, Pb^{2+}, and Al^{3+} was systematically investigated using colorimetric, UV–visible, and fluorescence spectroscopic techniques. Among the investigated dyes, azo dye 3b, (N-(4-methoxyphenyl)-2-hydroxy-1-[2-(5-nitro-2-benzoylphenyl) diazenyl] naphthalene-3-carboxamide), exhibited notable selectivity toward Pb^{2+} ions. Azo dye (3b) displayed an immediate naked-eye colour transition from green to nearly colourless upon interaction with Pb^{2+} ions. Job's plot analysis showed a 2:1 ligand-to-metal binding stoichiometry, while Benesi–Hildebrand analysis afforded an association constant of 2.0×10^{5} M^{-2}, suggesting strong binding affinity toward Pb^{2+} ions. The limit of detection and quantification were determined to be 1.21 μg mL^{-1} and 3.66 μg mL^{-1}, respectively. The present study demonstrates that azo dye 3b serves as a simple, rapid, selective, and efficient colorimetric chemosensor for Pb^{2+} ion detection with potential applicability in environmental monitoring systems.

Key words: Azo dye, Colorimetric chemosensor, Pb^{2+} detection.

1. Introduction

Contamination of water by heavy metal ions has become a major environmental and health problem worldwide (1-4). Among the toxic heavy metals, lead(II) ions (Pb^{2+}) are particularly dangerous because they can cause serious health problems even at very low concentrations (5-7). Pb^{2+} ions are widely used in industries such as battery manufacturing, paints, ceramics, mining, automobile production, and electroplating (8). Due to industrial discharge and other human activities, lead easily enters soil and water systems, causing long-term environmental pollution (9-13).

Exposure to Pb^{2+} can affect several organs and biological systems in humans (14). It may cause kidney damage, neurological disorders, anemia, cardiovascular problems, reproductive disorders, and developmental defects in children (15-17). Pb^{2+} ions can also interfere with enzyme activity, DNA transcription, and cell membrane function (18). Because of these harmful effects, the World Health Organization (WHO) has set the permissible limit of lead in drinking water at 10 μg L^{-1} (19). Therefore, the development of simple and reliable methods for Pb^{2+} detection is highly important.

Several instrumental techniques such as atomic absorption spectrometry (AAS) inductively coupled plasma mass spectrometry (ICP-MS), atomic fluorescence spectrometry (AFS), anodic stripping voltammetry (ASV), and X-ray fluorescence spectrometry (XRF) have been used for Pb^{2+} detection (20-29). Although these techniques are highly sensitive and accurate, they require costly instruments, complicated sample preparation, and skilled operators. These limitations make them less suitable for rapid and on-site monitoring.

In recent years, colorimetric chemosensors have attracted significant attention because they offer simple operation, fast response, low cost, and easy detection by the naked eye (30-34). Among different sensing materials, azo dyes are considered excellent candidates for colorimetric sensing due to their easy synthesis, strong visible absorption, and tunable optical properties (35-38). The presence of azo (–N=N–)

groups along with donor atoms such as oxygen and nitrogen enhances their ability to interact with metal ions, resulting in noticeable color changes (39-40).

Many azo dye-based chemosensors have been reported for the detection of toxic metal ions (41-42). However, ligands bind to metal ions through suitable donor atoms and form metal–ligand complexes. This binding can change the electronic properties of the ligand, which may result in a change in its absorption and colour. Functional groups such as hydroxyl, carbonyl, azo, and imine groups can provide binding sites for metal ions. Therefore, ligands containing such functional groups can be used to develop colorimetric chemosensors for the selective detection of metal ions. Azo-functionalized benzophenone-derived naphthalene systems for selective Pb^{2+} detection are still limited in the literature. Molecules containing hydroxyl, amide, carbonyl, nitro, and azo functional groups are expected to show strong coordination ability toward heavy metal ions and may produce significant optical responses upon binding.

In continuation of our research in the development of azo-based chemosensors, we report here the synthesis and sensing behaviour of a new azo dye, N-(4-methoxyphenyl)-2-hydroxy-1-[2-(5-nitro-2-benzoylphenyl)diazenyl]naphthalene-3-carboxamide, for the selective detection of Pb^{2+} ions. The sensing ability of the probe was investigated in the presence of different metal ions such as Fe^{2+}, Co^{2+}, Zn^{2+}, Hg^{2+}, Pb^{2+}, and Al^{3+}. Among all the tested metal ions, the probe showed a remarkable and selective response toward Pb^{2+} ions with a distinct colour change from green to nearly colourless, while other metal ions produced only negligible changes. This visible response indicates strong interaction between the probe and Pb^{2+} ions through coordination involving azo nitrogen and oxygen-containing functional groups. The present study demonstrates that the synthesized azo dye can act as a simple, rapid, and selective colorimetric chemosensor for Pb^{2+} detection.

2. Experimental

2.1. General information, materials and methods.

2-Amino-5-nitrobenzophenone (99% purity) was obtained from Sigma Aldrich and Bionova Supplies, Bangalore, Karnataka, India, and used directly for diazotization and coupling reactions without further purification. Other chemicals such as naphthol-ASOL, naphthol-Asbo and naphthol-AS were obtained from Bombay dyeing industries. And were recrystallized in acetone-water system before coupling reaction. sodium hydroxide, ferric chloride, cobalt chloride, mercuric chloride, and lead acetate were also used. All reagents were of analytical grade and purchased from SRL Chemicals and Nice Chemicals, India.

The progress of the reactions was monitored using thin-layer chromatography (TLC) on aluminium-backed silica gel 60 F_{254} plates, and the spots were observed under UV light. UV–visible spectra of the synthesized azo dyes were recorded using a HITACHI UH-5300 spectrophotometer in the range of 200–800 nm. Infrared (IR) spectra were obtained using a BRUKER ALPHA-II FT-ATIR spectrophotometer in the range of 500–4000 cm^{-1}. The ^{1}H NMR and ^{13}C NMR spectra were recorded on a VARIAN FT-NMR spectrometer operating at 400 MHz. Mass spectra were recorded using a 1260 INFINITY II PRIME LC/MSD iQ plus instrument.

2.2 Synthesis

2.2.1 Preparation of azo dye 3a-3c

Azo dyes 3a–3c were synthesized via a conventional diazotization–coupling reactions. 2-Amino-5-nitrobenzophenone 0.1g (0.411mmol) was dissolved in hydrochloric acid and the solution was cooled to 0 °C. A precooled aqueous solution of sodium nitrite 0.02g, (0.28 mmol) was added dropwise over 10 min under continuous stirring, while maintaining the temperature at 0–5 °C, to generate the corresponding diazonium chloride. The diazonium solution was maintained at this temperature to ensure stability. Subsequently, diazonium salt was added slowly to an alkaline solution of

naphthol-ASBO 0.128g(0.57mmol). at 0–5 °C, the reaction mixture was kept on stirring for 2-3hrs resulting in the formation of azo dye 3a. Azo dyes 3b and 3c were synthesized similarly by coupling the diazonium intermediate with appropriate coupling components, namely naphthol-ASOL 0.11g(0.375mmol) and naphthol-AS 0.108g(0.4101mmol). respectively, under identical experimental conditions.

The precipitates obtained were isolated by filtration, washed thoroughly with cold water, and air-dried. Further purification was achieved by recrystallization from an acetone–water system. The structures of the synthesized azo dyes were confirmed by spectroscopic studies.

Dye code	**Dye name**	**Colour**	**% Yield**	**Solubility**
3a	4-[(E)-(2,3-dihydro-1H-inden-5-yl)diazenyl]naphthalen-1-ol	Pink	76	DMF/DMSO
3b	1-[(E)-(2,3-dihydro-1H-inden-5-yl)diazenyl]naphthalen-2-ol	Orange	80	DMF/DMSO
3c	6-bromo-1-[(E)-(2,3-dihydro-1H-inden-5-yl)diazenyl]naphthalen-2-ol	Peach	83	DMF/DMSO

Table-1: Physical properties, percentage yield, colour, and solubility of the synthesized azo dyes (3a–3c).

2.2 Stock Solution Preparation for Chemosensing Studies

2.2.1 Dye Stock Solution

Stock solutions of azo dyes 3b and 3c (5.0×10^{-4} M) were prepared by dissolving the respective compounds in dimethylsulphoxide (DMSO). For spectroscopic measurements, an aliquot (5 mL) of the stock solution was diluted to 100 mL with DMSO to obtain a working concentration of 2.50×10^{-5} M. These solutions were employed for UV–visible and fluorescence studies.

2.3.2 Metal Salt Solution

Metal ion solutions (1.5×10^{-3} M) were prepared by dissolving the appropriate metal salts in deionized water, followed by dilution to a final volume of 100 mL.

2.3 UV–Vis Spectroscopic Evaluation of Metal Ion Selectivity

Upon addition of the metal ions, the solutions were gently mixed and allowed to equilibrate for 3 min at room temperature prior to spectral investigations. All measurements were performed using DMSO as the reference solvent. Among the investigated dyes, compound 3b exhibited a distinct and selective response toward Pb^{2+} ions; consequently, further sensing studies were focused on the 3b-Pb^{2+}.

2.4 UV–Visible and Fluorescence Spectroscopic Titration Analysis

The interaction between azo dye 3b and Pb^{2+} ions was examined using UV–visible and fluorescence spectroscopy in DMSO. For UV–visible titrations, a solution of azo dye 3b (2.50×10^{-5} M, 3.0 mL) was titrated with Pb^{2+} ions (1.50×10^{-3} M) in a 1 cm quartz cuvette. After each incremental addition, the solution was mixed and equilibrated for 3 min at room temperature prior to recording the spectra. Absorption measurements were carried out using DMF as the reference.

Fluorescence studies were performed under analogous conditions by recording the emission spectra of azo dye 3b (2.50×10^{-5} M) in the absence and presence of Pb^{2+} ions to evaluate the effect of metal ion binding on the emission properties of the dye.

2.5 Determination of Binding Stoichiometric ratio via Job's plot method.

To determine the binding stoichiometry between the synthesized azo dye and Pb^{2+} ions, a Job's plot (method of continuous variations) analysis was carried out. Equimolar solutions of the azo dye (2.5×10^{-5} M) and Pb^{2+} (1.5×10^{-3} M) were prepared in ethanol. A series of mixtures was obtained by varying the volume ratios of dye and metal ion, while maintaining a constant total volume of 3 mL for each sample.

The resulting solutions were mixed thoroughly and allowed to equilibrate at room temperature. The absorbance spectra were recorded using a UV–Vis spectrophotometer, and the absorbance values corresponding to the complex formation band (≈370 nm) were noted. The corrected absorbance values were plotted against the mole fraction of the azo dye to construct the Job's plot.

2.6 Determination of association constant

The association constant (K_a) for the interaction between azo dye 3b and Pb^{2+} ions was determined using the Benesi–Hildebrand method. A solution of azo dye 3b (2.50×10^{-5} M, 3.0 mL) in DMSO was titrated with lead(II) ions (1.50×10^{-3} M), and the absorption spectra were recorded using UV–visible spectrophotometry. After each addition, the solution was mixed thoroughly and allowed to equilibrate for 3 min at room temperature prior to measurement.

The association constant was calculated using the Benesi–Hildebrand equation:

$$\frac{1}{A-A_0} = \frac{1}{K_a(A_{\max}-A_0)[M^{2+}]^2} + \frac{1}{A_{\max}-A_0} \quad (1)$$

where A_0represents the absorbance of the free receptor (azo dye 3b) in the absence of Pb^{2+} ions, A is the absorbance after each incremental addition of Pb^{2+}, and $A_{\max}$ corresponds to the absorbance at saturation. The association constant (K_a, M^{-1}) was obtained from the slope of the linear plot of $1/(A - A_0)$versus $1/[Pb^{2+}]^2$.

2.7 Calculation of the Limit of Detection (LOD)

The limit of detection (LOD) for azo dye 3b toward Pb^{2+} ions was determined based on the IUPAC 3σ criterion using UV–visible spectrophotometry with a 1 cm path-length quartz cuvette. The absorbance of a blank solution of azo dye 3b (2.50×10^{-5} M, 3.0 mL) in DMSO was recorded at least five times to estimate the standard deviation (SD) of the blank signal.

Subsequently, the same solution was titrated with lead(II) ions (1.50×10^{-3} M), and the absorption spectra were recorded after each incremental addition following equilibration for 3 min at room temperature. A calibration curve was constructed by plotting absorbance against the corresponding Pb^{2+} ion concentration within the linear range.

The LOD was calculated using the following expressions:

$$\mathrm{LOD} = 3\sigma \quad (2)$$

$$\sigma = \frac{\mathrm{SD}}{s} \quad (3)$$

where SD represents the standard deviation of the blank measurement and s is the slope of the calibration curve.

3. Results and discussions

Scheme-1 illustrates the synthesis of a series of azo dyes (3a–3c). The formation of intensely coloured precipitates indicates the successful formation of chromophoric (-N=N-) azo bond. The completion of reaction and products were monitored by thin-layer chromatography (TLC) and subsequently purified by recrystallization. Structural confirmation of the synthesized dyes was achieved through comprehensive spectroscopic analyses. The spectral data obtained were in full agreement with the proposed molecular structures.

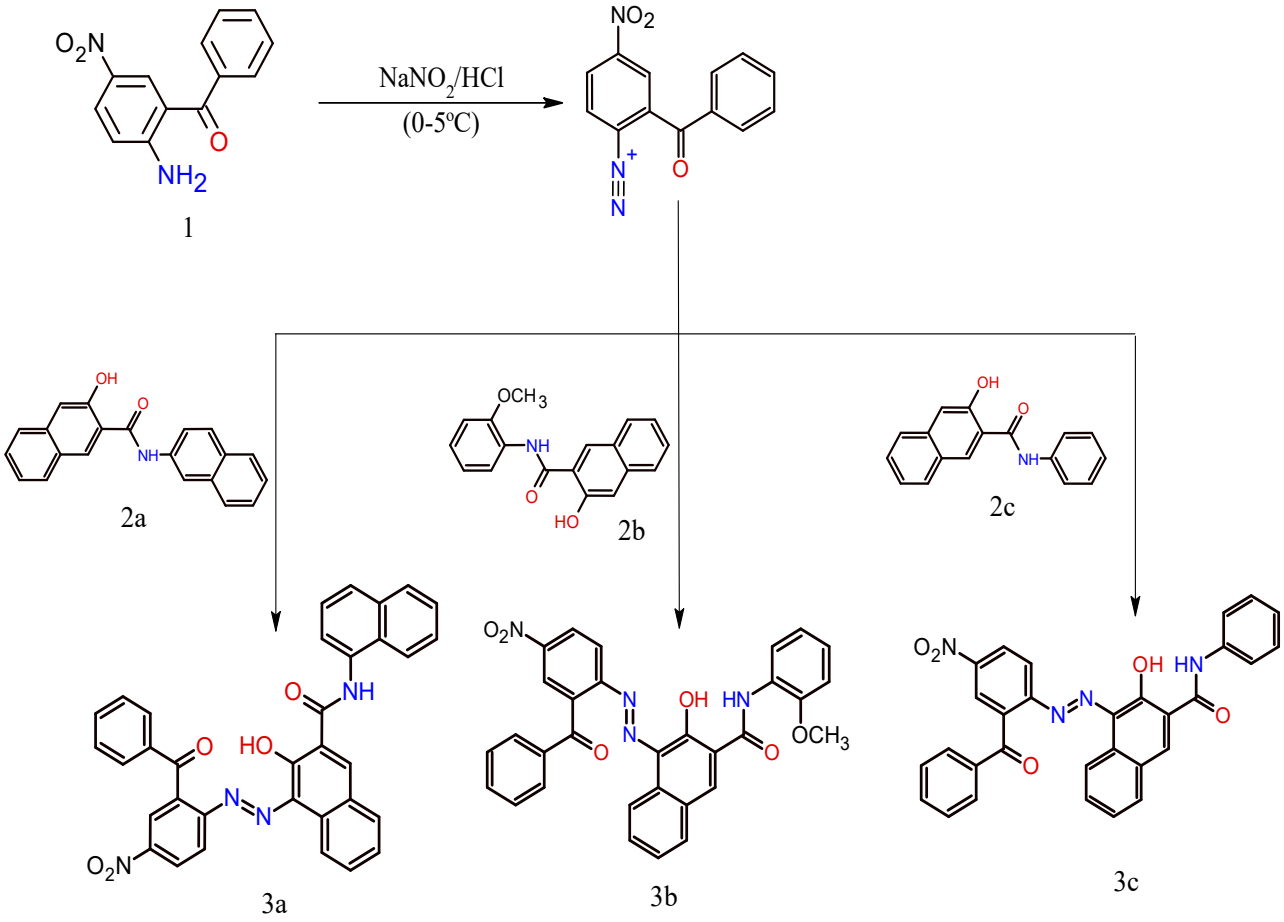

Scheme-1: Synthetic route of azo dye 3a-3c

3.1 Spectral characterization

The synthesized compounds were successfully characterized to confirm their chemical structures using various spectroscopic techniques, including UV–Visible, FT-IR, ^{1}H NMR, ^{13}C NMR, and mass spectrometry. The spectral data obtained from these analyses were in good agreement with the proposed molecular structures and are discussed in the following sections.

Compound 3a: UV–Vis (λmax, nm): 262, 337. FT-IR (ν, cm^{-1}): 3450 (O–H), 3243 (N–H), 3058 (Ar–H), 1628 (C=O), 1556 (N=N), 1503 (NO_2, asymmetric), 1350 (NO_2, symmetric), 1247 (C–O). ^{1}H NMR (400 MHz, DMSO-d_6, δ, ppm): 11.34 (s, 1H, OH), 10.60 (s, 1H, NH), 6.99–8.51 (m, Ar–H). ^{13}C NMR (100 MHz, DMSO-d_6, δ, ppm): 196.70 (C=O), 165.64, 156.22, 153.73, 153.54, 138.45, 134.48, 131.89, 131.81, 130.47, 128.82, 128.71, 128.57, 126.86, 126.13, 125.77, 124.06, 123.48, 121.79, 120.96, 114.64, 110.55 (Ar–C). MS (m/z): 566.0 [M].

Compound 3b: UV–Vis (λmax, nm): 261, 370. FT-IR (ν, cm^{-1}): 3447 (O–H), 3330 (N–H), 3167 (Ar–H), 1697 (C=O), 1590 (NO_2, asymmetric), 1560 (N=N), 1375 (NO_2, symmetric), 1246 (C–O). ^{1}H NMR (400 MHz, DMSO-d_6, δ, ppm): 12.63 (s, 1H, OH), 10.26 (s, 1H, NH), 7.02–8.20 (m, Ar–H), 3.80 (s, 3H, OCH_3). ^{13}C NMR (100 MHz, DMSO-d_6, δ, ppm) 136.431, 136.068, 135.884, 134.483, 133.346, 131.855, 131.561, 131.157, 130.534, 130.337, 130.135, 129.868, 128.807, 128.538, 128.379, 128.277, 128.140, 127.475, 127.005, 126.878, 126.483, 126.306, 125.705, 124.851, 123.816, 123.238, 120.905, 117.073, 116.775, 114.608, 110.728, 110.585. MS (m/z): 547.0 $[M+H]^+$.

Compound 3c: UV–Vis (λ_max, nm): 268, 369, 613. FT-IR (ν, cm^{-1}): 3447 (O–H), 3331 (N–H), 2975 (C–H), 1617 (C=O), 1559 (N=N), 1478 (NO_2, asymmetric), 1362 (NO_2, symmetric), 1249 (C–O). ^{1}H NMR (400 MHz, DMSO-d_6, δ, ppm): 11.10 (s, 1H, OH), 8.75 (s, 1H, NH), 8.21–6.91 (m, Ar–H). ^{13}C NMR (100 MHz, DMSO-d_6, δ, ppm): 196.694, 165.471, 156.207, 153.862, 138.532, 134.951, 134.487, 133.731, 133.239, 131.874, 131.460, 131.169, 128.909, 128.813, 128.554, 128.463, 128.338, 127.245, 127.052, 126.393, 126.168, 125.786, 125.455, 123.875, 123.750, 122.091, 120.991, 120.795, 114.628, 110.794. MS (m/z): 514.9 $[M]^+$

3.2 Colorimetric chemosensor studies

3.2.1 Response time of azo dyes 3b–3c toward metal ions

The response time of azo dyes 3b and 3c toward the selected metal ions was evaluated by monitoring their spectroscopic changes in solution. Solutions of azo dyes 3b-3c (2.5×10^{-5} M) were prepared in DMSO, followed by the addition of respective metal ions, and the variation in absorbance intensity was recorded.

Furthermore, the response of azo dye 3b toward Pb^{2+} ions was also investigated using fluorescence spectroscopy under similar experimental conditions. In all cases, both the absorbance of azo dyes 3b-3c and the fluorescence intensity of azo dye 3b exhibited a rapid change immediately after the addition of metal ions and reached a stable plateau within 3 minutes. Based on these observations, an incubation time of 3 minutes was considered sufficient and was consistently maintained in all subsequent experiments to ensure complete interaction between the azo dyes and the metal ions.

3.2.2 Colorimetric Sensing and UV–Visible Studies

The interaction of azo dyes 3b–3c with various metal ions (Fe^{2+}, Co^{2+}, Zn^{2+}, Hg^{2+}, Pb^{2+} and Al^{3+}). in DMSO was investigated using colorimetric and UV–visible spectroscopic methods. Solutions of the azo dyes (2.5×10^{-5} M) were treated individually with four equivalents of the respective metal ions and the resulting colour changes were recorded after 15 minutes.

Azo dye 3b, showed a green colour (fig-16). Upon addition of Fe^{2+}, the solution turned deeper shade of green. With Co^{2+}, Hg^{2+}, and Al^{3+} ions, the solutions also retained the green colour, indicating no significant colour change. In contrast, when Pb^{2+} was added, the solution showed a clear change from green to nearly colourless, which is distinctly different from all other metal ions. This strong decolorization confirms the selective detection of Pb^{2+} by 3b.

Azo dye 3c, the blank solution exhibited a blue colour (fig-17). Upon addition of Fe^{2+}, the solution turned light blue, while Co^{2+} resulted in a slightly deeper blue shade. In the presence of Hg^{2+}, the solution showed a noticeable change to a more intense blue,

and with Pb^{2+}, a moderate blue shade was observed. Similarly, Al^{3+} produced a blue color with slight variation in intensity. Although the colour remained blue in all cases, the intensity differences were clearly visible, indicating non-selective interactions with the tested metal ions.

Overall azo dye 3b shows a distinct and selective colour change in the presence of Pb^{2+}, whereas 3c exhibits sensitivity to all metal ions, indicating a non-selective responsive behaviour.

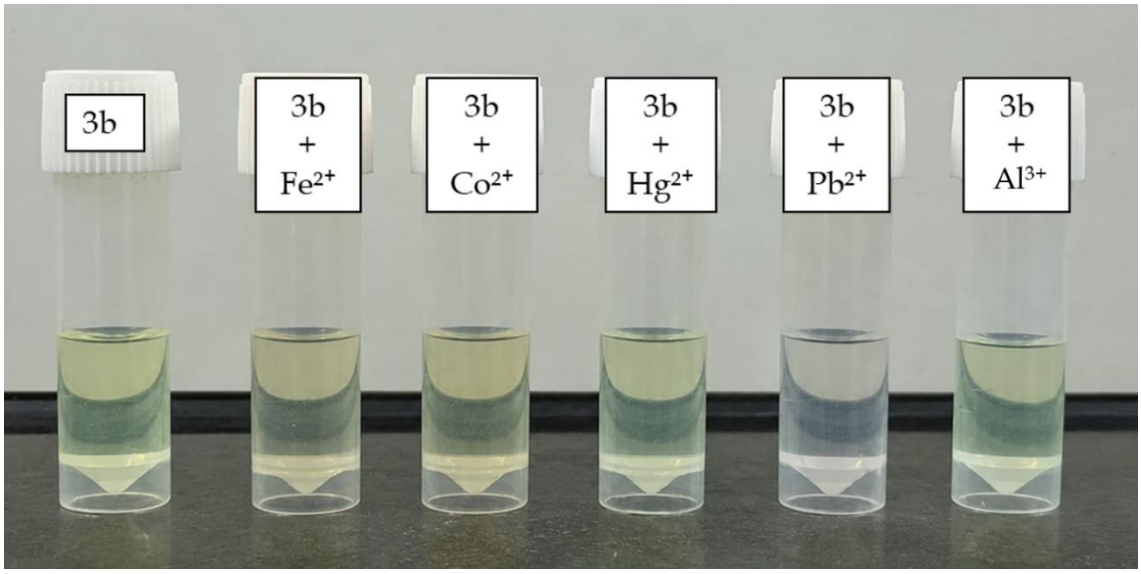

Figure-16: Colour change of azo dye 3b (2.5×10^{-5}M) upon addition of metal ions

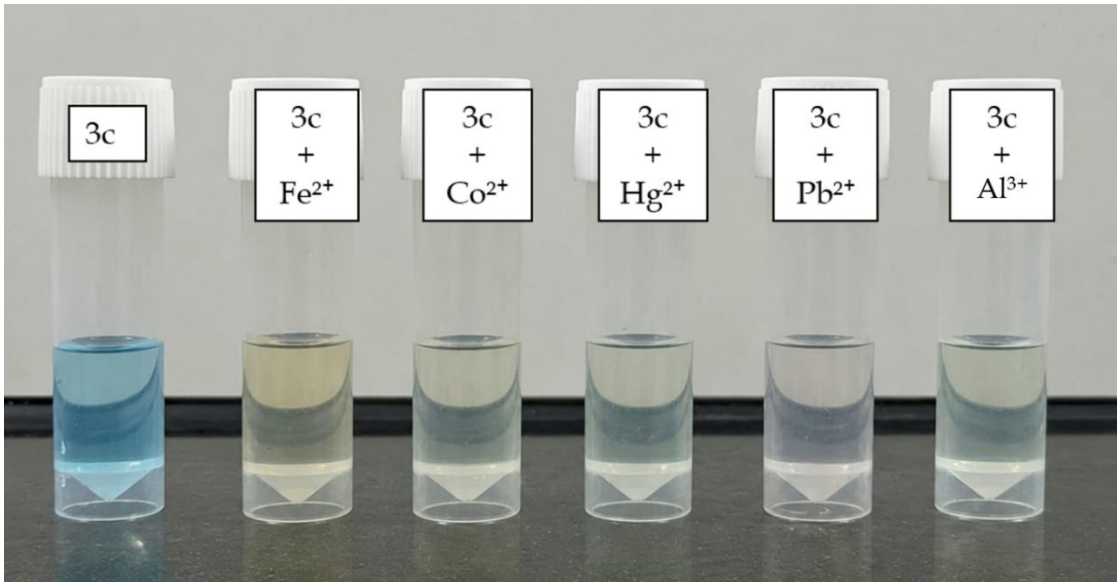

Figure-17: Colour change of azo dye 3c (2.5×10^{-5}M) upon addition of metal ions

To further evaluate selectivity, UV–visible absorption spectra of azo dyes 3b-3c (2.5×10^{-5} M) were recorded after the addition of four equivalents of metal ions. As shown in (fig-18), azo dye 3b displayed an absorption band at 337 nm, which showed small bathochromic shifts to 339 nm in the presence of Fe^{2+} ions, while no significant spectral shift was observed with Co^{2+}, $Hg^{2+}$and Al^{3+} ions. Notably, the addition of Pb^{2+} resulted in the hypsochromic shift of band 332nm along with a visible colour change. This distinct spectral feature indicates a specific interaction and strong binding affinity of 3b toward Pb^{2+} ions.

In the case of azo dye 3c minor spectral changes were observed (fig-19). A slight shift in the absorption maximum from 370 nm to ~367 nm was observed with Fe^{2+} and Pb^{2+}, while Co^{2+}, Hg^{2+} and Al^{3+} caused moderate bathochromic shift to 375nm. The absence of a clear and consistent spectral pattern confirms the non-selective behaviour of 3c.

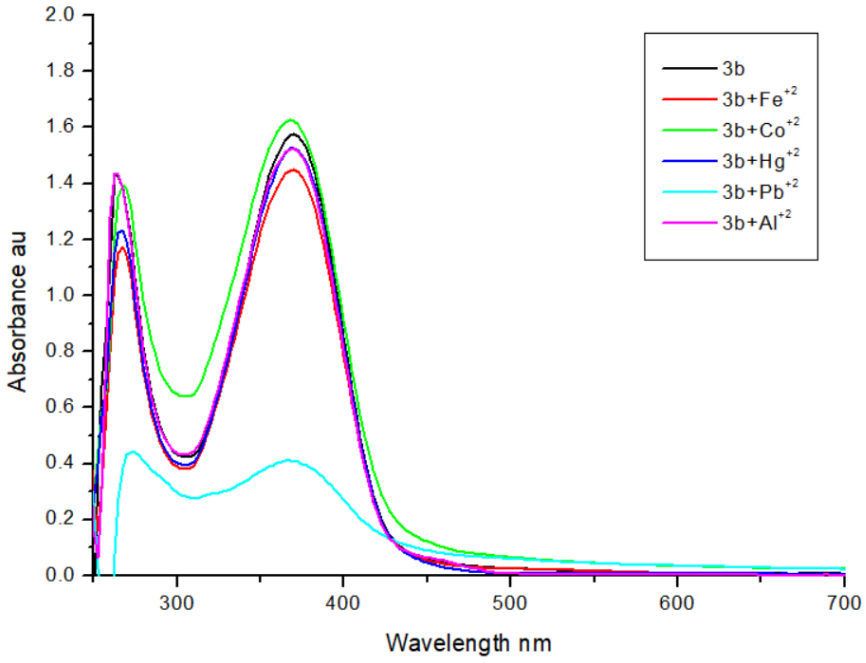

Figure-18: UV-Vis Spectra of azo dye 3b (2.5×10^{-5}M) upon addition of metal ions.

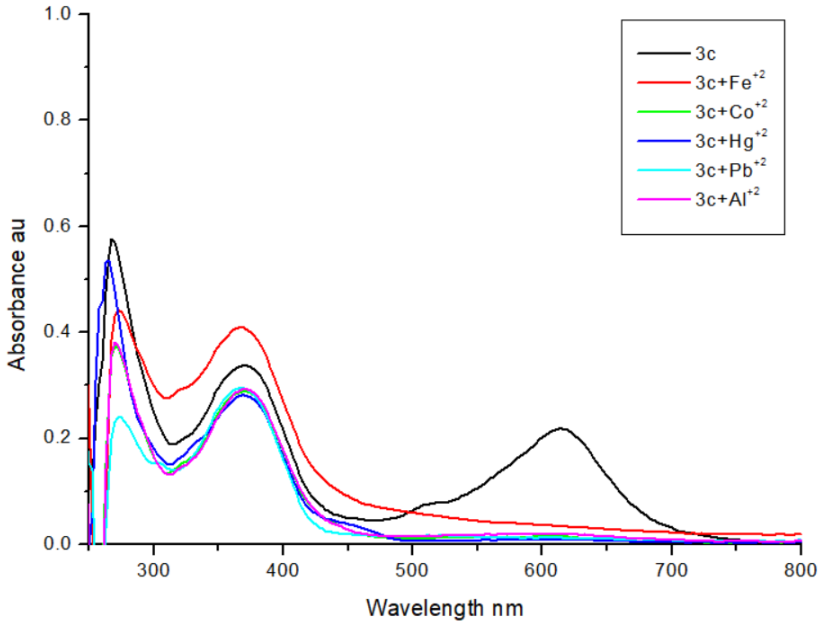

Figure-19: UV-Vis Spectra of azo dye 3c (2.5 x 10^{-5}M) upon addition of metal ions.

The UV–visible absorption spectrum of azo dye 3b exhibited a prominent absorption band at 365 nm with a molar absorptivity of $6.0 \times 10^4\ M^{-1}cm^{-1}$, which can be attributed to the π→π* transition of the azo chromophore (fig-20). Another absorption band observed around 600 nm is associated with n→π* transition. Upon addition of Pb^{2+} ions, the absorbance intensity of the main band significantly decreased, and the molar absorptivity reduced to $1.6 \times 10^4\ M^{-1}cm^{-1}$along with slight band broadening, indicating the formation of a Pb^{2+}–azo dye 3b complexation.

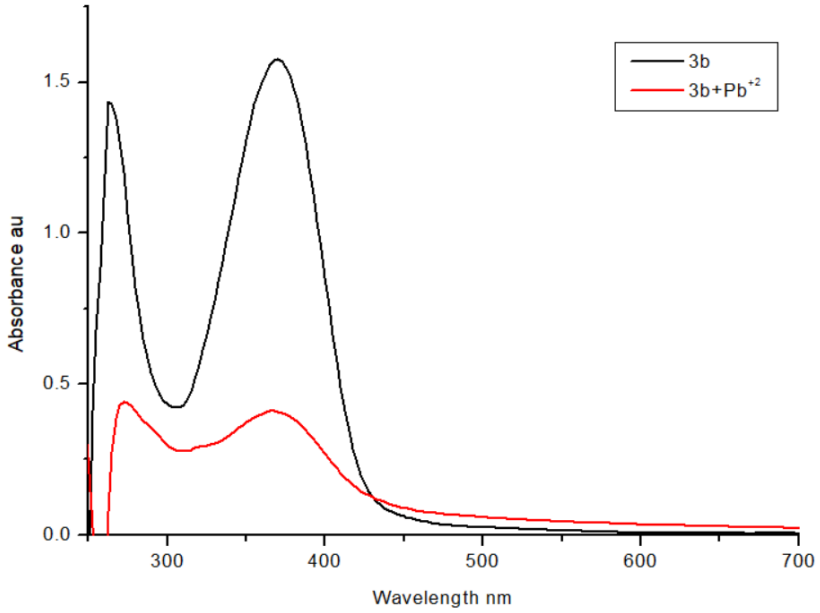

Figure-20: Uv-vis spectra of azo dye 3b (2.5×10^{-5}M) in the absence and presence of Pb^{+2} ion.

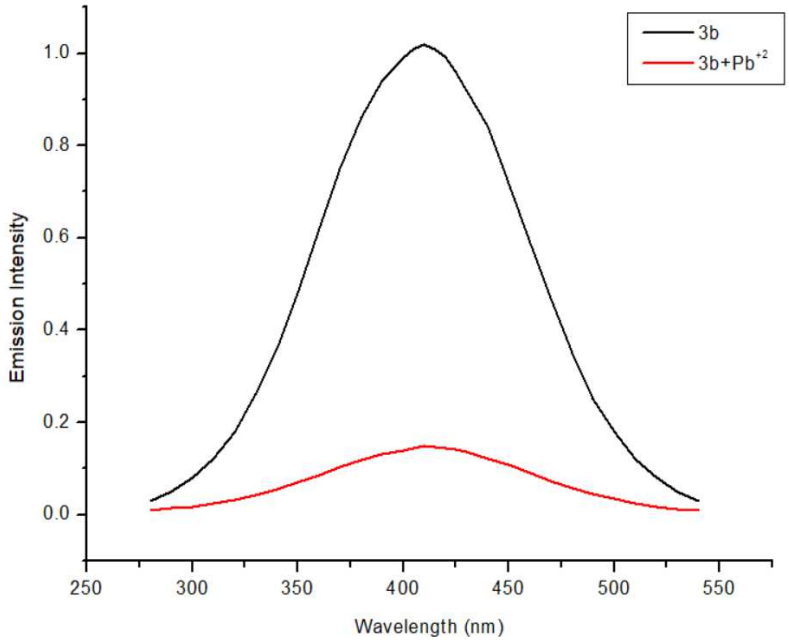

Figure-21: Fluroscence spectra of azo dye 3c (2.5×10^{-5}M) in the absence and presence of Pb^{+2} ion.

Furthermore, the fluorescence emission behaviour of azo dye 3b was investigated in the absence and presence of Pb^{2+} ions. Upon excitation, the free dye exhibited a strong emission band centred around 410 nm with an emission intensity of approximately 1.0 au

(fig-21). The addition of Pb^{2+} ions resulted in pronounced fluorescence quenching, reducing the emission intensity to nearly 0.15 au without significant shift in the emission maximum. The marked decrease in fluorescence intensity indicates strong interaction between Pb^{2+} ions and azo dye 3b, suggesting the formation of a stable Pb^{2+}–azo dye complex and suppression of the excited-state emission process.

4.1.3 Job's Plot experiment

To elucidate the binding stoichiometry between the synthesized azo dye 3b and Pb^{2+} ions, a Job's plot of continuous variations was constructed by monitoring the absorbance at ~370 nm across a series of solutions with varying mole fractions of dye and Pb^{2+} (fig-22). The plot displayed a clear maximum at a mole fraction of the azo dye of approximately 0.62, beyond which the absorbance gradually decreased, indicating saturation of the complex formation.

This maximum corresponds to a 2:1 binding stoichiometry (3b: Pb^{2+}), suggesting that two ligand molecules coordinate to a single Pb^{2+} ion. This behaviour is consistent with the ability of Pb^{2+} to accommodate multiple donor atoms and form stable complexes with azo dye ligands. The suggested azo dye 3b- Pb^{+2} complex structure is as shown in the (fig-23).

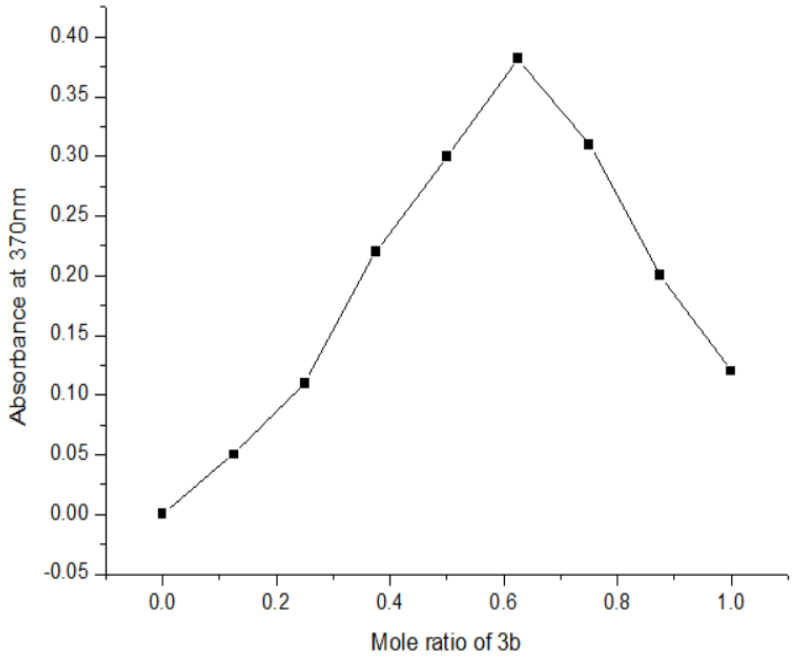

Figure-22: Job's plot to determine the binding stoichiometry between azo dye 3b and Pb^{+2} .

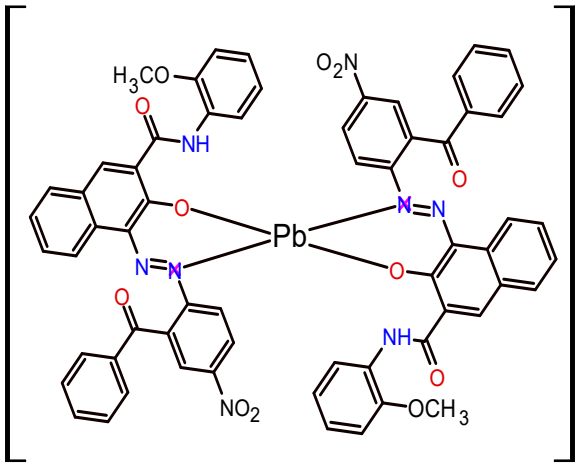

Figure-23: The suggested azo dye 3b- Pb^{+2} complex structure.

4.1.4 Binding Affinity Studies of Azo Dye towards Pb^{2+} Ions.

To gain further insight into the interaction between the synthesized azo dye and Pb^{2+} ions, the binding affinity was evaluated using a modified Benesi–Hildebrand equation assuming a 2:1 (L_2M) stoichiometric ratio. The plot of $1/(A - A_0)$ versus $1/[Pb^{2+}]^2$ exhibited excellent linearity with a correlation coefficient of $R^2 = 0.9989$, confirming the validity of the applied model (fig-24). The linear regression equation was found to be $y = 4.927 \times 10^{-6}x + 1.0129$. The high degree of linearity supports the formation of a well-defined complex, consistent with the 2:1 stoichiometry obtained from Job's plot analysis. The association constant (K_a), calculated from the slope of the plot, was found to be 2.0×10^5 M^{-2}, indicating strong binding affinity of the azo dye towards Pb^{2+} ions. The relatively high binding constant suggests efficient coordination between the ligand and Pb^{2+}, which may be attributed to the presence of donor sites such as azo nitrogen (–N=N–) and other heteroatoms such as -OH within the ligand framework, facilitating stable complex formation.

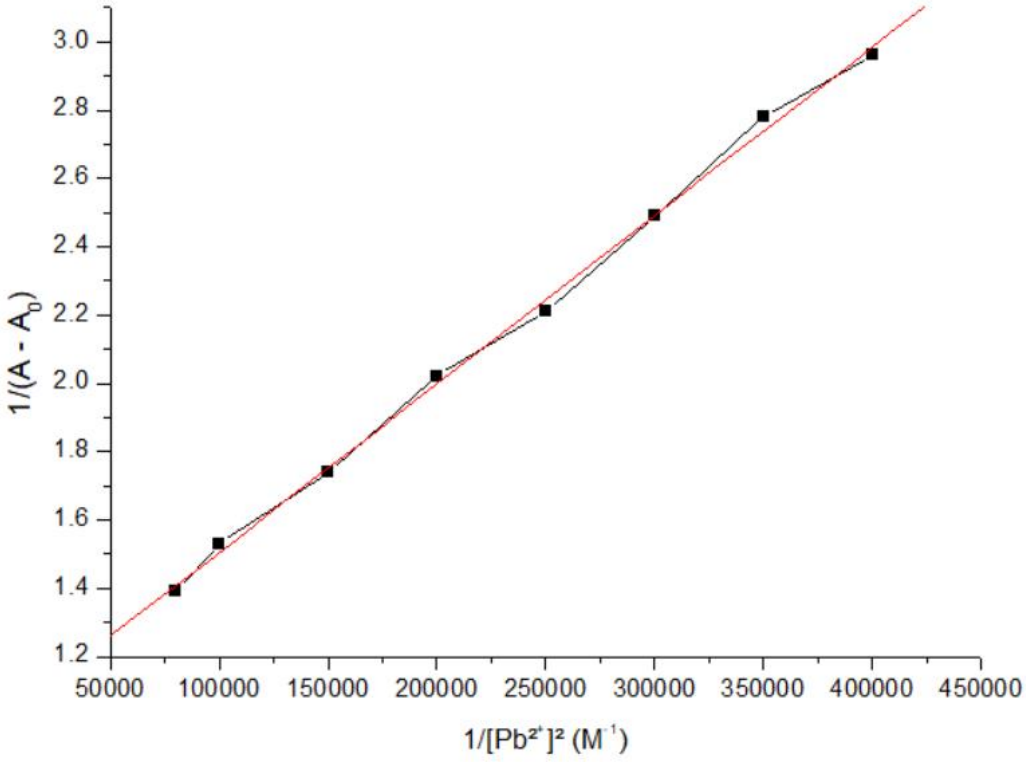

Figure-24: Benesi–Hildebrand plot showing the linear relationship between $1/(A - A_0)$and $1/[Pb^{2+}]^2$.

4.1.5 Analytical Performance Limit of Detection and Quantification Studies.

The limit of detection (LOD) of the present azo dye toward Pb^{2+} ions was calculated from the UV–visible calibration data using the standard deviation (σ = 0.0046 AU) and the slope of the calibration curve (S = 0.01258 AU μg^{-1} mL). The LOD and limit of quantification (LOQ) were determined to be 1.21 µg mL^{-1} and 3.66 µg mL^{-1}, respectively (fig-25). These values indicate good sensitivity for Pb^{2+} detection within the studied concentration range. The obtained LOD is comparable with reported azo dye systems, where anthracene-based azo dyes exhibit LOD values of ~7.5 µM (≈1.5 µg mL^{-1}) [43], and azobenzene-derived systems show LOD values around ~5.44 µM [44]. In this context, the LOD and LOQ obtained in the present study gives good detection limit as simple colorimetric azo dye sensors, confirming its practical applicability while also suggesting scope for further sensitivity enhancement through structural modification or incorporation of fluorogenic units.

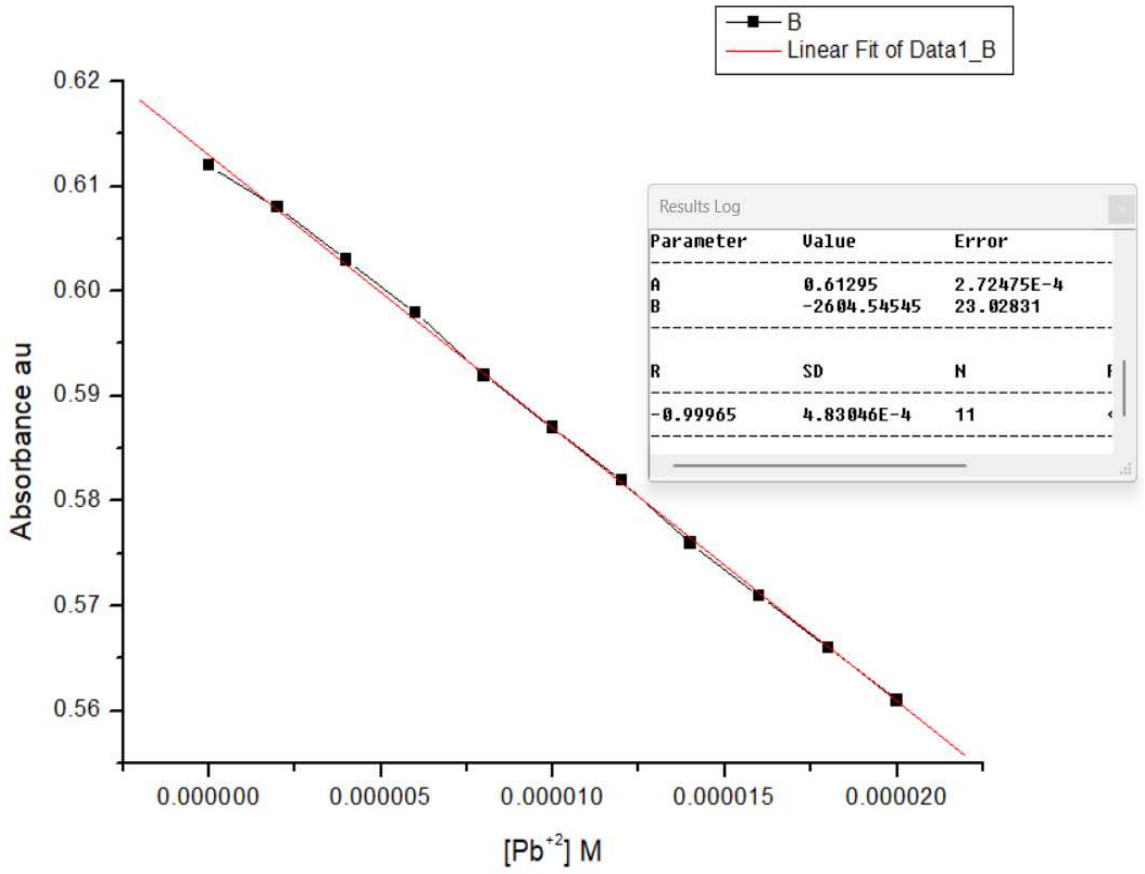

Figure-25: Calibration plot showing the variation in absorbance of azo dye 3b with increasing Pb^{2+} concentration.

Conclusion.

A series of benzophenone-derived azo dyes (3a–3c) were successfully synthesized through conventional diazotization–coupling reactions and characterized using spectroscopic techniques. The synthesised dyes were evaluated for their chemosensor selectivity towards heavy metal ions (Fe^{2+}, Co^{2+}, Zn^{2+}, Hg^{2+}, Pb^{2+} and Al^{3+}). azo dye 3b exhibited exceptional selectivity toward Pb^{2+} ions, producing an immediate and distinct colour transition from green to nearly colourless, which enabled naked-eye detection. UV–visible spectroscopic studies revealed significant modulation in the electronic absorption behaviour of the dye upon addition of Pb^{2+}, characterized by a decrease in absorbance intensity and reduction in molar absorptivity, confirming 3b-Pb^{2+} complexation. Fluorescence studies demonstrated efficient quenching of the emission band in the presence of Pb^{2+} ions. Job's plot analysis established a 2:1 ligand-to-metal stoichiometric ratio, while Benesi–Hildebrand treatment indicated a high association constant (2.0×10^5 M^{-2}), demonstrating strong binding affinity between azo dye 3b and Pb^{2+} ions. Low detection limit of 1.21 μg mL^{-1} confirms the good analytical sensitivity of the developed sensing system toward Pb^{2+} ions.

The present work highlights the potential of benzophenone-derived azo chromophores as efficient moieties for heavy metal ion sensing. Synthesised azo dye 3b possesses efficient synthetic accessibility, rapid sensing, strong binding affinity and good selectivity toward Pb^{2+} ions, establishing its potential as an effective colorimetric chemosensor for sensitive and reliable detection of lead contamination in environmental and analytical systems.

Acknowledgement:

The laboratory facilities provided by Davangere University's Department of Chemistry are warmly acknowledged by the authors. The University Sophisticated Instrumentation Centre is also acknowledged by the authors for providing access to FTIR and UV-Vis equipment. The ^1H NMR and LC-MS data were provided by Spark Analytical, for which one of the writers is truly grateful. For help with computational

research, the authors are grateful to Dr Ranganath Kamath of the Chemistry Department of research at Presidency University Bengaluru.

Declarations

Funding

Funding

No funding was received for this research.

Ethics approval and consent to participate

This study is not applicable because it does not involve the use of animals or humans. Not applicable.

Competing interests

The authors declare no competing interests.

Data availability

The datasets generated during and/or analysed during the current study are available from the corresponding author on reasonable request.

Reference.

1. Dhirendra Kumar Chaudhary, Anil Sharma, Ambreesh Kumar, Upendra Chauhan, Hari P. Bhasker, D. P. K. Dhawan, & Shiv P. Patel. (2022). Solvent engineering of $Cs_3Bi_2I_9$ perovskite films for lead-free flexible semi-transparent perovskite solar cell devices with enhanced efficiency. SSRN Electronic Journal. https://doi.org/10.2139/ssrn.4226736
2. Gall, J. E., Boyd, R. S., & Rajakaruna, N. (2015). Transfer of heavy metals through terrestrial food webs: A review. Environmental Monitoring and Assessment, 187(4), 201. https://doi.org/10.1007/s10661-015-4436-3
3. Violante, A., Cozzolino, V., Perelomov, L., Caporale, A. G., & Pigna, M. (2010). Mobility and bioavailability of heavy metals and metalloids in soil environments. Journal of Soil Science and Plant Nutrition, 10(3), 268–292. https://doi.org/10.4067/S0718-95162010000100005
4. Gupta, N., Khan, D. K., & Santra, S. C. (2008). An assessment of heavy metal contamination in vegetables grown in wastewater-irrigated areas of Titagarh, West Bengal, India. Bulletin of Environmental Contamination and Toxicology, 80(2), 115–118. https://doi.org/10.1007/s00128-007-9327-z
5. Gunnlaugsson, T., Kruger, P. E., Jensen, P., Tierney, J., Ali, H. D. P., & Hussey, G. M. (2005). Colorimetric "naked eye" sensing of anions in aqueous solution. The Journal of Organic Chemistry, 70(26), 10875–10878. https://doi.org/10.1021/jo0520487
6. Kaur, B., Kaur, N., & Kumar, S. (2018). Colorimetric metal ion sensors: A comprehensive review of the years 2011–2016. Coordination Chemistry Reviews, 358, 13–69. https://doi.org/10.1016/j.ccr.2017.12.002
7. Lin, S. H., & Juang, R. S. (2002). Heavy metal removal from water by sorption using surfactant-modified montmorillonite. Journal of Hazardous Materials, 92(3), 315–326. https://doi.org/10.1016/S0304-3894(02)00026-2
8. Elgarahy, A. M., Elwakeel, K. Z., Mohammad, S. H., & Elshoubaky, G. A. (2021). A critical review of biosorption of dyes, heavy metals and metalloids from wastewater as an efficient and green process. Case Studies in Chemical and Environmental Engineering, 4, 100209. https://doi.org/10.1016/j.cscee.2021.100209
9. Aragay, G., Pons, J., & Merkoçi, A. (2011). Recent trends in macro-, micro-, and nanomaterial-based tools and strategies for heavy-metal detection. Chemical Reviews, 111(5), 3433–3458. https://doi.org/10.1021/cr100383r

10. Kongor, A., Panchal, M., Athar, M., Makwana, B., Sindhav, G., Jha, P. C., & Jain, V. (2018). Synthesis and modeling of calix[4]pyrrole wrapped Au nanoprobe for specific detection of Pb(II): Antioxidant and radical scavenging efficiencies. Journal of Photochemistry and Photobiology A: Chemistry, 364, 801–810. https://doi.org/10.1016/j.jphotochem.2018.07.024
11. He, W., Luo, L., Liu, Q., & Chen, Z. (2018). Colorimetric sensor array for discrimination of heavy metal ions in aqueous solution based on three kinds of thiols as receptors. Analytical Chemistry, 90(7), 4770–4775. https://doi.org/10.1021/acs.analchem.8b00076
12. Ferreira de Mattos, G., Costa, C., Savio, F., & Alonso, M. (2017). Lead poisoning: Acute exposure of the heart to lead ions promotes changes in cardiac function and Cav1.2 ion channels. Biophysical Reviews, 9(5), 807–825. https://doi.org/10.1007/s12551-017-0303-5
13. Gupta, N., Khan, D. K., & Santra, S. C. (2008). An assessment of heavy metal contamination in vegetables grown in wastewater-irrigated areas of Titagarh, West Bengal, India. Bulletin of Environmental Contamination and Toxicology, 80(2), 115–118. https://doi.org/10.1007/s00128-007-9327-z
14. Briffa, J., Sinagra, E., & Blundell, R. (2020). Heavy metal pollution in the environment and its toxicological effects on humans. Heliyon, 6(9), e04691. https://doi.org/10.1016/j.heliyon.2020.e04691
15. Flora, S. J. S., Flora, G., & Saxena, G. (2006). Environmental occurrence, health effects and management of lead poisoning. In J. S. Casas & J. Sordo (Eds.), Lead: Chemistry, analytical aspects, environmental impacts and health effects (Vol. 4, pp. 158–228). Elsevier. https://doi.org/10.1016/B978-044452945-9/50004-X
16. Wu, H. M., Lin-Tan, D. T., Wang, M. L., Huang, H. Y., Lee, C. L., Wang, H. S., Lin, C. Y., Huang, Y. L., & Lin, J. L. (2012). Lead level in seminal plasma may affect semen quality for men without occupational exposure to lead. Reproductive Biology and Endocrinology, 10(1), 91. https://doi.org/10.1186/1477-7827-10-91
17. Bellinger, D. C. (2005). Teratogen update: Lead and pregnancy. Birth Defects Research Part A: Clinical and Molecular Teratology, 73(6), 409–420. https://doi.org/10.1002/bdra.20127
18. Yedjou, C. G., Tchounwou, C. K., Haile, S., Edwards, F., & Tchounwou, P. B. (2010). N-acetyl-cysteine protects against DNA damage associated with lead toxicity in HepG2 cells. Ethnicity & Disease, 20(1 Suppl 1), S1-101–S1-103.

19. World Health Organization. (2011). Guidelines for drinking-water quality (4th ed.). World Health Organization.
20. Çaylak, O., Elçi, Ş. G., Höl, A., Akdoğan, A., Divrikli, Ü., & Elçi, L. (2019). Use of an aminated Amberlite XAD-4 column coupled to flow injection cold vapour generation atomic absorption spectrometry for mercury speciation in water and fish tissue samples. Food Chemistry, 274, 487–493. https://doi.org/10.1016/j.foodchem.2018.08.107
21. Lynam, M. M., Klaue, B., Keeler, G. J., & Blum, J. D. (2013). Using thermal analysis coupled to isotope dilution cold vapor ICP-MS in the quantification of atmospheric particulate phase mercury. Journal of Analytical Atomic Spectrometry, 28(11), 1788–1795. https://doi.org/10.1039/C3JA50184A
22. Zhao, S. L., Chen, F. S., Zhang, J., Ren, S. B., Liang, H. D., & Li, S. S. (2015). On-line flame AAS determination of traces Cd(II) and Pb(II) in water samples using thiol-functionalized SBA-15 as solid phase extractant. Journal of Industrial and Engineering Chemistry, 27, 362–367. https://doi.org/10.1016/j.jiec.2015.01.015
23. Billon, G., & van den Berg, C. M. G. (2004). Gold and silver micro-wire electrodes for trace analysis of metals. Electroanalysis, 16(19), 1583–1591. https://doi.org/10.1002/elan.200302990
24. Rani, P., Lal, K., & Shrivastava, R. (2019). Tris-triazole based chemosensors for selective sensing of Pb^{2+} ions. Asian Journal of Chemistry, 31(11), 2443–2447. https://doi.org/10.14233/ajchem.2019.22076
25. Munksgaard, N. C., Batterham, G. J., & Parry, D. L. (1998). Lead isotope ratios determined by ICP-MS: Investigation of anthropogenic lead in seawater and sediment from the Gulf of Carpentaria, Australia. Marine Pollution Bulletin, 36(7), 527–534. https://doi.org/10.1016/S0025-326X(97)00183-1
26. Cave, M. R., Butler, O., Cook, J. M., Cresser, M. S., Garden, L. M., & Miles, D. L. (2000). Environmental analysis. Journal of Analytical Atomic Spectrometry, 15(2), 181–235. https://doi.org/10.1039/A908001D
27. Cave, M. R., Butler, O., Chenery, S. R., Cook, J. M., Cresser, M. S., & Miles, D. L. (2001). Atomic spectrometry update. Environmental analysis. Journal of Analytical Atomic Spectrometry, 16(2), 194–235. https://doi.org/10.1039/B006502P

28. Wilschefski, S. C., & Baxter, M. R. (2019). Inductively coupled plasma mass spectrometry: Introduction to analytical aspects. The Clinical Biochemist Reviews, 40(3), 115–133. https://www.ncbi.nlm.nih.gov/pmc/articles/PMC6839093/
29. M. Shamsipur, L. Farzin, M.A. Tabrizi, S. Sheibani, Functionalized Fe 3 O 4 oxide nanocomposites with hairpin aptamers for the separation and preconcentration of trace Pb 2+ /graphene from biological samples before determination by ICP MS, Mater. Sci. Eng. C 77 (2017) 459–469, https://doi.org/10.1016/j. msec.2017.03.262.
30. S. Ozdemir, E. Kilinc, K.S. Celik, V. Okumus, M. Soylak, Simultaneous preconcentrations of Co 2+ , Cr 6+ , Hg 2+, and Pb 2+ ions by Bacillus altitudinis immobilized nanodiamond prior to their determinations in food samples by ICP- OES, FoodChem. 215 (2017) 447–4453, https://doi.org/10.1016/j. foodchem.2016.07.055
31. H. Rahimi, R. Hosseinzadeh, M. Tajbakhsh, A new and efficient pyridine-2, 6-dicarboxamide-based fluorescent and colorimetric chemosensor for sensitive and selective recognition of Pb 2+ and Cu 2+ , J. Photochem. Photobiol. A Chem. 407 (2021), 113049 https://doi.org/10.1016/j.jphotochem.2020.113049
32. M.A. Satam, R.K. Raut, N. Sekar, Fluorescent azo disperse dyes from 3-(1, 3-ben zothiazole-2-yl) naphthalene-2-ol and comparison with 2-naphthol analogs, Dyes Pigm. 96 (2013) 92–103, https://doi.org/10.1016/j.dyepig.2012.07.019
33. H. Li, Z. Xiong, X. Dai, Q. Zeng, The effect of perspiration on the photo-induced chemical reaction of azo dyes and the determination of aromatic amine products, Dyes Pigm. 94 (2012) 55–59, https://doi.org/10.1016/j.dyepig.2011.11.006
34. Sancenón, F., Martínez-Máñez, R., Miranda, M. A., Seguí, M. J., & Soto, J. (2003). Towards the development of colorimetric probes to discriminate between isomeric dicarboxylates. Angewandte Chemie International Edition, 42(6), 647–650. https://doi.org/10.1002/anie.200390178
35. Sola, A., Tárraga, A., & Molina, P. (2012). A ferrocenyl-guanidine derivative as a highly selective electrochemical and colorimetric chemosensor molecule for acetate anions. Dalton Transactions, 41(28), 8401–8409. https://doi.org/10.1039/C2DT30632H
36. G. Dhaka, N. Kaur, J. Singh, Spectral studies on benzimidazole-based "bare-eye" probe for the detection of Ni 2+ : Application as a solid-state sensor, Inorg. Chim. Acta 464 (2017) 18–22, https://doi.org/10.1016/j.ica.2017.04.042
37. S. Ghosh, P. Jana, K. Ghosh, A naphthalimide-linked new pyridylazo phenol derivative for selective sensing of cyanide ions (CN) in sol–gel medium, Anal. Methods 13 (2021) 695–702, https://doi.org/10.1039/D0AY02033H

38. A. Battison, S. Schoeman, N. Mama, A coumarin-azo derived colorimetric chemosensor for Hg detection in organic and aqueous media and its extended real-world applications, 2022. https://doi.org/10.21203/rs.3.rs-1621696/v1
39. Towns, A. D. (1999). Developments in azo disperse dyes derived from heterocyclic diazo components. Dyes and Pigments, 42(1), 3–28. https://doi.org/10.1016/S0143-7208(99)00005-4
40. M.A. Weaver, L. Shuttleworth, Heterocyclic diazo components, Dyes Pigm. 3 (1982) 81–121, https://doi.org/10.1016/0143-7208(82)80016-8
41. Ghorbanian, M., Asghari, S., & Tajbakhsh, M. (2023). A new benzothiazole azo dye colorimetric chemosensor for detecting Pb^{2+} ion. Spectrochimica Acta Part A: Molecular and Biomolecular Spectroscopy, 296, 122652. https://doi.org/10.1016/j.saa.2023.122652
42. Wang, Y. T., Hu, S., Zhang, Y., Gong, H., Sun, R., Mao, W., & Chen, Y. (2018). A colorimetric Pb^{2+} chemosensor: Rapid naked-eye detection, high selectivity, theoretical insights, and applications. Journal of Photochemistry and Photobiology A: Chemistry, 355, 101–108. https://doi.org/10.1016/j.jphotochem.2017.10.027
43. Olaleye, S. O., & Bibi, U. (2025). A new azo dye for colorimetric determination of lead(II) ions. RSC Advances, 15(26), 20770–20780. https://doi.org/10.1039/D5RA02486B
44. Ghorbanian, M., Asghari, S., & Tajbakhsh, M. (2023). A new benzothiazole azo dye colorimetric chemosensor for detecting Pb^{2+} ion. Spectrochimica Acta Part A: Molecular and Biomolecular Spectroscopy, 296, 122652. https://doi.org/10.1016/j.saa.2023.122652